Simultaneous Estimation of the Phase Content and Lamellar Thickness in Isotactic Polypropylene by the Simulated Annealing of Wide-Angle X-Ray Scattering Data

Gopinath Subramanian,[1] Rahmi Ozisik[2]

[1]*Scientific Computation Research Center, Rensselaer Polytechnic Institute, 110 8th Street, Troy, New York 12180*
[2]*Department of Materials Science and Engineering, Rensselaer Polytechnic Institute, 110 8th Street, Troy, New York 12180*

Received 21 November 2009; accepted 8 January 2010
DOI 10.1002/app.32079
Published online 13 April 2010 in Wiley InterScience (www.interscience.wiley.com).

ABSTRACT: Wide-angle X-ray scattering (WAXS) patterns of isotactic polypropylene (iPP) were analyzed in terms of the ideal WAXS patterns of their individual phases. Analysis was done with the technique of simulated annealing. This analysis is a novel method for simultaneously obtaining the volume fractions of the crystalline and amorphous phases and the average lamellar thickness of the individual crystalline phases. The method is different from traditional methods as it allowed us to obtain a large amount of information in a single step from a single WAXS pattern. This study was limited to a few selected specimens of iPP, but the method expounded could, in principle, be extended to other polymers and polymer blends. The limits of its applicability and possible shortcomings are discussed.
 J Appl Polym Sci 117: 2386–2394, 2010

Key words: isotactic; lamellar; polymorphism; polypropylene (PP); WAXS

INTRODUCTION

Polymers are a versatile material used in multiple applications in the form of fibers, films, coatings, and bulk material. Their versatility arises in part because of the complex structural organization of the chains, which results in a variety of microstructures. The ability to control the microstructure with different processing techniques is a widely used method for tuning the bulk material properties of any finished product. One aspect of the microstructure that is of interest is its crystallinity. Polymers are known to form semicrystalline structures that are denser and tougher than their amorphous counterparts; this makes them attractive for use in many industries. In the interests of quality control or the development of a processing methodology, it is of practical interest to measure the overall crystallinity. From a fundamental standpoint, the current theories of polymer crystallization and dynamics have been investigated with crystallinity measurements.[1–4] Microanalysis techniques, such as wide-angle X-ray scattering (WAXS), density measurements, and differential scanning calorimetry (DSC), are routinely used in both industry and academia to measure crystallinity.

Another aspect of crystalline polymers that is of interest is their lamellar size. Polymer crystals grown from solution at low growth rates have a relatively small number of defects. In melt crystallization, when the growth rate is high, complex sheaflike or spherical lamellar aggregates are formed.[5] The nature of these aggregates depends on the lamellar size and has a profound impact on the mechanical properties of the resulting bulk material. The amorphous region between spherulites is thought to be weaker and less dense than the crystalline domains; thus serving as a site for crack propagation[6–11] and dielectric breakdown.[12–16] DSC measurements have been used to estimate the lamellar thickness, and DSC has been found to be extremely sensitive to the heating rates and parameters in the Gibbs–Thomson equation, and thus, unsuitable as a tool for routine quantitative analysis.[17] Lamellar thickness is, thus, typically measured with more advanced techniques, such as transmission electron microscopy,[18–20] small-angle X-ray scattering (SAXS),[20–23] and atomic force microscopy.[24–26]

Some polymers, such as poly(ethylene oxide), are capable of forming only one type of crystalline phase.[27,28] Other polymers have the ability to form multiple crystalline phases. Examples of the latter include the α, β, and γ phases of isotactic

Correspondence to: G. Subramanian (gsub@scorec.rpi.edu).

polypropylene (iPP)[29–31] and the orthorhombic and hexagonal phases of polyethylene.[32] The output of many of the aforementioned microanalysis techniques is a composite of the contributions from the individual components that make up the polymer specimen being examined. In techniques such as DSC, whereas in principle, it may be possible to decompose the experimental signal into contributions from the individual components, experimental difficulties make it hard to do so. In WAXS, on the other hand, the contributions of the individual components to the composite scattered beam can, in a significant number of cases, be clearly distinguished,[33,34] and form the basis of qualitative phase identification.

In a polymer specimen such as iPP, in addition to qualitative information, it is of both practical and fundamental interest to obtain quantitative information about the (1) relative fractions of the amorphous and crystalline (α, β, and γ) phases, (2) lamellar size, and (c) degree of crystallinity. The relative content of the individual phases may be obtained from a WAXS pattern with the Turner–Jones method,[35] where, for example, the fraction of the α phase is computed from the heights of the most prominent peaks of each phase (i.e., H_α, H_β, and H_γ) as $H_\alpha/(H_\alpha + H_\beta + H_\gamma)$. The degree of crystallinity has been obtained from WAXS patterns in a variety of ways.[2,36–39] In these methods, one deconvolutes the amorphous halo from the crystalline peaks by obtaining the WAXS pattern of a purely amorphous specimen or a melt.[40] The maximum intensity of the normalized amorphous pattern, and selected intensities of crystalline peaks from the test specimen are, then, combined in a variety of correlations[41–45] to yield the degree of crystallinity. One may obtain the most probable lamellar thickness by converting SAXS data into the well-known long spacing using Bragg's law and combining this with the degree of crystallinity obtained with DSC or WAXS.[17,20,21]

Although many techniques available in the literature extract information from WAXS patterns that is pertinent to the work being performed (e.g., crystallinity, fraction of the α phase), what has been lacking is a general-purpose algorithm that is capable of extracting a large amount of information from a single WAXS pattern. In this paper, we aim to elucidate a method for simultaneously obtaining the degree of crystallinity, relative phase fraction, and most probable lamellar thickness of each phase. To this end, the WAXS pattern of a test specimen was analyzed in terms of its constituent elements. Although in this study we examined iPP in particular, the method expounded is general and can be extended to any polymer system or system of polymer blends. The applicability and limitations of this technique are also discussed in detail.

METHODS

The WAXS pattern to be analyzed is denoted as $\Psi(2\theta)$. It is assumed to be a composite of the contributions from the individual phases, which, in the case of iPP, are one amorphous and three crystalline phases. As evidenced by the work of Krache et al.,[46] Nedkov and Dobreva,[47] Busse and Kressler,[48] and Addink and Bientema,[49] all four phases can coexist. In fact, Addink and Bientema[49] discovered the γ phase of iPP by analyzing the WAXS patterns of iPP that contained all four phases. The contributions from each component were assumed to be independent of each other. Under these assumptions, an experimentally obtained WAXS pattern can be decomposed as follows:

$$\Psi(2\theta) = \phi_A \psi_A(2\theta) + \sum \phi_i \psi_i(2\theta, L_i). \quad (1)$$

where $\Psi(2\theta)$ is the integrated experimental WAXS pattern, $\psi_A(2\theta)$ is the WAXS pattern of the amorphous phase, ϕ_i is the volume fraction of phase i (where $i = A$, α, β, and γ), and $\psi_i(2\theta,L_i)$ is the WAXS pattern of the pure crystalline phase (where L_i is the lamellar thickness of the crystalline phase i, and θ is the Bragg angle).

In eq. (1), the weighting factors (ϕ_i) were chosen to be the volume fractions instead of weight fractions because, in an X-ray scattering experiment, the probability with which the incident beam strikes a given phase is assumed to be the volume fraction of that phase. The individual WAXS patterns, ψ_i and Ψ, were treated as probability density functions and were subjected to the following normalization conditions:

$$\int \psi_i(2\theta, L_i) d(2\theta) = 1; \; i = \alpha, \beta, \gamma. \quad (2)$$

$$\int \psi_A(2\theta) d(2\theta) = 1. \quad (3)$$

$$\int \Psi(2\theta) d(2\theta) = 1. \quad (4)$$

The WAXS pattern of amorphous iPP was obtained from experimental data on elastomeric iPP.[50] A Pseudo-Voigt function was fitted to the experimental data, and this fit was considered to be the WAXS pattern of the purely amorphous phase.

The unit cell dimensions and fractional coordinates of the carbon atoms of the α, β, and γ phases were obtained from the literature.[29–31,33,34,51–54] With this information, structures were built with commercial software Materials Studio, a product developed by Accelerys, Inc.[55] The Reflex module of the software was then used to compute the structure factors and, thereby, the position (as a function of 2θ) and the relative intensity of the powder diffraction peaks

TABLE I
Peak Positions and Relative Intensities of Ideal iPP Obtained with the Ideal Crystal Structures

α phase		β phase		γ phase	
2θ (°)	Intensity	2θ (°)	Intensity	2θ (°)	Intensity
14.150	1.000	16.050	1.000	8.340	0.010
16.900	0.696	16.500	0.025	13.840	1.000
18.550	0.652	21.100	0.349	15.050	0.143
21.250	0.299	23.100	0.071	16.720	0.796
21.850	0.431	24.650	0.048	17.230	0.122
24.450	0.030	28.000	0.061	18.350	0.000
25.200	0.033	28.250	0.028	20.070	0.755
25.500	0.050	29.000	0.021	21.220	0.388
27.150	0.049	31.250	0.076	21.880	0.673
28.450	0.051	31.350	0.031	23.350	0.000
28.550	0.048	31.950	0.011	24.350	0.051
29.100	0.048	35.350	0.016	25.200	0.112
29.250	0.021	36.600	0.020	26.950	0.010
29.750	0.017	42.750	0.027	27.550	0.005
29.875	0.015	42.850	0.011	27.660	0.005
32.700	0.017	43.550	0.020	27.880	0.010
32.850	0.017			28.830	0.122
33.300	0.040			29.010	0.031
33.400	0.015			29.630	0.000
33.675	0.041			29.690	0.000
34.900	0.061			30.370	0.010
35.850	0.011			33.350	0.010
36.900	0.025			34.620	0.014
37.000	0.020			34.690	0.014
37.550	0.010			34.750	0.014
38.575	0.022				
41.100	0.014				
41.450	0.011				
42.400	0.017				
42.500	0.051				
42.600	0.025				
42.800	0.024				
42.900	0.014				
43.150	0.041				
43.250	0.029				
44.200	0.016				
44.300	0.021				
44.500	0.011				
44.600	0.015				

of each of the crystalline phases. The values used in this study are reproduced in Table I.

We incorporated the effect of the lamellar thickness by treating each peak as a Gaussian function with the height as determined previously and with the full width at half-maximum determined with the Scherrer equation,[56,57] as follows:

$$w = \frac{K\lambda}{L\cos\theta}. \quad (5)$$

where w is the full width at half-maximum of a peak; K is the Scherrer constant, taken to be 0.93 in this study;[56] λ is the X-ray wavelength; and L is the lamellar thickness.[58,59]

More complex functions, such as pseudo-Voigt, Pearson VII, and Voigt[60,61] have been used to account for the line broadening of the WAXS data. We chose to use the Gaussian function because, as a two-parameter function, it was mathematically simpler and was a reasonable approximation to the WAXS peaks. Furthermore, the accuracy that is gained with more complex functions may not be necessary for purposes of this study, and as will be seen in the following sections, the Gaussian performed exceedingly well. Lattice strain also contributes to line broadening of a WAXS peak, which was not explicitly accounted for in this study. Thus, for specimens with lattice strain, the lamellar thickness predicted by simulated annealing is expected to be a lower limit.

Thus, by the proper choice of variables ϕ_i and L_i, we sought to minimize the error function (E) defined as follows:

$$E(\phi_\alpha, L_\alpha, \phi_\beta, L_\beta, \phi_\gamma, L_\gamma, \phi_A) = \int [\Psi(2\theta) - \phi_A\psi_A(2\theta) - \sum\nolimits_i \psi_i(2\theta, L_i)]^2 d2\theta. \quad (6)$$

The minimization of E in eq. (6) is a constrained minimization problem. To solve this problem, we chose the technique of simulated annealing,[62] which is an adaptation of the Metropolis–Hasting algorithm for global optimization, and is described briefly. A schematic of the method is shown in Figure 1.

The phase space for the system under consideration is the space defined by seven variables as $S(\phi_\alpha,\phi_\beta,\phi_\gamma,\phi_A,L_\alpha,L_\beta,L_\gamma)$, subjected to the following constraints:

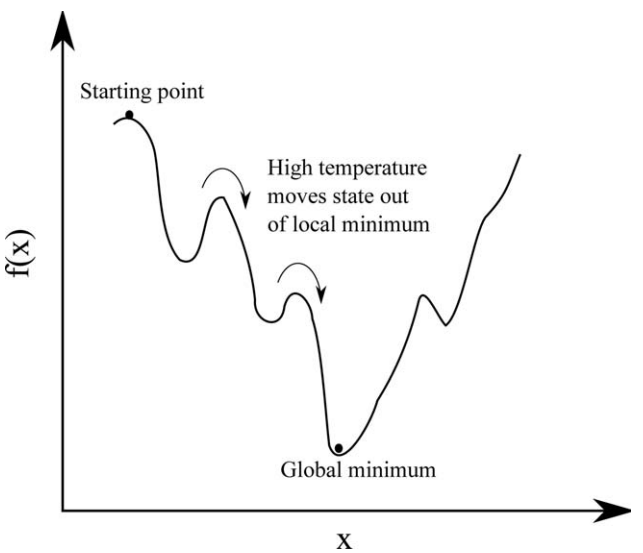

Figure 1 Schematic representation of simulated annealing for a function [$f(x)$] having as its phase space the single variable x. The starting point was chosen at random. A high temperature allowed the system to escape from local minima.

$$0 \leq \phi_i \leq 1, i = \alpha, \beta, \gamma, A. \quad (7)$$

$$0 \leq L_i \leq L_{max}, i = \alpha, \beta, \gamma. \quad (8)$$

$$\phi_\alpha + \phi_\beta + \phi_\gamma + \phi_A = 1. \quad (9)$$

Strictly speaking, L_{max}, the maximum lamellar thickness, is unbounded. However, from a practical standpoint, it is extremely rare to obtain lamellae thicker than about 500 Å,[17–26,63–65] and thus, the maximum lamellar thickness was fixed as twice that value, at 1000 Å.

The technique of simulated annealing begins with choosing a state (S_j) at random in the phase space defined previously. The error function $E(S_j)$ is evaluated at this point. A trial new state (S_{j+1}) is generated as $S_{j+1} = S_j + \Delta S_j$. Downhill moves, or moves that decrease the value of E, are always accepted, and uphill moves, or moves that increase the value of E, are accepted with a probability [$P(T)$] given by the Metropolis criterion. Thus, the probability with which the trial state is accepted is given by

$$P(T) = min\left\{1, \exp\left[\frac{E_j - E_{j+1}}{\tilde{T}}\right]\right\}. \quad (10)$$

where $\tilde{T}$ is called the temperature of the system. At the start of a simulated annealing run, the temperature was assigned a value of unity and changed as $\tilde{T}_{new} = 0.9\tilde{T}_{old}$ after every 20 evaluations of E. This choice was made after extensive trial and error and allowed the simulated annealing runs to complete in a reasonable amount of time and the state of the system to escape from local minima. We believe that this choice is specific to the iPP system being considered.

To validate the method presented previously, experimental WAXS data of iPP was obtained from the literature. We chose the work of Mezghani and Philips[34] and Broda,[66–68] as these articles have presented extensive sets of WAXS data, along with independent measurements of the phase content (ϕ_i) and lamellar thickness (L_i). As is customary, these articles have reported WAXS data on an arbitrary intensity scale. In situations where multiple sets of WAXS data are presented in the same figure, the curves are shifted by an unspecified amount toward higher intensities for the sake of readability. To overcome the effect of the unknown shift factor, all WAXS curves obtained from the literature [denoted as $\Psi'(2\theta)$] were shifted downward, such that the lowest intensity value of each curve was zero. Thus, the curves used as input to the simulated annealing routine were obtained as follows:

$$\Psi(2\theta) = \Psi'(2\theta) - \min(\Psi'(2\theta)). \quad (11)$$

This transformation of the experimental data effectively reduces the contribution of the amorphous halo to the diffractogram, and thus, was expected to result in an underestimation of ϕ_A of the test specimen and to leave the volume fractions of the crystalline phases relative to each other unchanged. We believe that a WAXS pattern that is corrected for instrument broadening but without the amorphous halo removed can be used directly with this method. The lamellar thicknesses (L_i values) were also expected to be unaffected, except perhaps in the case of extremely low crystalline content material, as the transformation does not change the width of the crystalline peaks.

Each transformed experimental WAXS pattern was analyzed multiple times, each time with a different random seed. A small number of seeds resulted in the reporting of a local minimum as a global minimum, as evidenced by the discrepancy between the experimental data and the fit. Such results were discarded, and a different random seed was chosen. The volume fraction and lamellar thickness of each phase were then averaged over the results of nine different seeds that were not discarded.

RESULTS AND DISCUSSION

The first comparison between experiment and fitting was made with WAXS data published by Broda.[66–68] These experiments have been described in great detail elsewhere[66] and are briefly summarized here. Mosten 52.945, a commercial iPP with a narrow molecular weight distribution and a melt flow index of 2.5 g/min, was extruded from the melt at two different temperatures, 210 and 250°C, into air at 20°C. Fibers were spun at seven different take-up velocities, ranging from 100 to 1350 m/min. Noncolored and colored fibers were produced. Colored fibers were produced by the addition of 0.5 wt % quinacridone pigment just before fiber formation. Each of these 28 specimens was powdered on a Hardy microtome into segments of approximately 12.5 μm. WAXS patterns were obtained with an X-ray diffractometer (HZG-4) in the 2θ range 5–35°. SAXS data was obtained with an MBraun small and wide angle X-ray scattering camera with a Kratky collimating system. SAXS data was collected in the 2θ range 0–5°.

Tables II and III summarize the most probable lamellar thickness of the individual phases and their volume fractions, as obtained from simulated annealing for each of the experimental WAXS patterns. To compare these data with the lamellar thicknesses obtained with independent SAXS

TABLE II
Summary of the Most Probable Lamellar Thickness of Each Phase Obtained from Simulated Annealing

	Extrusion velocity (m/min)	L_i (Å)					
		210°C			250°C		
		α	β	γ	α	β	γ
Noncolored	100	101 ± 7	29 ± 16	32 ± 2	132 ± 1	7 ± 1	29 ± 5
	200	96 ± 10	23 ± 17	51 ± 9	79 ± 2	12 ± 2	33 ± 3
	300	94 ± 14	11 ± 3	51 ± 7	11 ± 1	34 ± 2	87 ± 9
	400	81 ± 10	21 ± 10	48 ± 10	11 ± 4	61 ± 4	35 ± 2
	880	105 ± 18	13 ± 5	34 ± 5	103 ± 2	107 ± 3	83 ± 7
	1050	86 ± 9	19 ± 9	38 ± 4	40 ± 12	39 ± 13	52 ± 13
	1350	109 ± 7	22 ± 14	41 ± 6	96 ± 7	8 ± 1	33 ± 2
Colored	100	28 ± 9	127 ± 8	55 ± 11	14 ± 5	99 ± 5	59 ± 14
	300	101 ± 6	61 ± 12	32 ± 8	89 ± 10	20 ± 5	46 ± 4
	400	106 ± 13	17 ± 8	63 ± 11	94 ± 11	9 ± 2	57 ± 12
	880	81 ± 9	29 ± 15	66 ± 13	87 ± 10	26 ± 10	52 ± 9
	1050	61 ± 7	15 ± 8	70 ± 10	78 ± 10	13 ± 4	50 ± 8
	1350	99 ± 6	9 ± 2	43 ± 9	92 ± 8	19 ± 8	43 ± 3

measurements,[66] the overall most probable lamellar thickness ($\langle L \rangle$) was then computed as a weighted average of the individual lamellar thicknesses as follows:

$$\langle L \rangle = \frac{\sum_{i=\alpha,\beta,\gamma} \phi_i L_i}{\sum_{i=\alpha,\beta,\gamma} \phi_i}. \quad (12)$$

Figure 2 shows a plot of $\langle L \rangle$ as a function of the extrusion velocity for the different specimens. The experimentally obtained lamellar thicknesses were in the range 25–80 Å. With the exception of one outlier, the predictions from simulated annealing also fell in the same range. Because of the small range and size of the error bars, it is difficult to determine whether $\langle L \rangle$ increases or decreases with take-up velocity. The lamellar thicknesses determined with simulated annealing seem to be slightly lower than the thickness determined by SAXS, indicating that the specimens might have contained some residual lattice strain.

The amorphous content obtained from simulated annealing was in the range 20–34% for all specimens. These values seem unrealistically low, and this is a consequence of the baseline correction that was employed in eq. (11). Thus, a direct comparison between crystallinity indices is not possible. However, the content of the crystalline phases relative to each other is expected to match values obtained by other measurement techniques.

TABLE III
Summary of the Volume Fraction of Each Phase Obtained from Simulated Annealing for Noncolored Fibers and Fibers Colored with Quinacridone

	Extrusion velocity (m/min)	210°C					250°C				
		ϕ_α	ϕ_β	ϕ_γ	ϕ_A	ϕ_A^E	ϕ_α	ϕ_β	ϕ_γ	ϕ_A	ϕ_A^E
Noncolored	100	28 ± 3	12 ± 2	37 ± 3	21 ± 2	48	18 ± 2	25 ± 2	31 ± 9	24 ± 5	59
	200	21 ± 2	21 ± 2	29 ± 2	26 ± 3	60	11 ± 4	21 ± 3	33 ± 1	34 ± 6	68
	300	15 ± 2	21 ± 3	35 ± 2	28 ± 1	66	31 ± 3	6 ± 2	29 ± 5	31 ± 2	82
	400	15 ± 2	24 ± 4	35 ± 3	24 ± 3	68	43 ± 6	5 ± 1	31 ± 3	19 ± 7	90
	880	15 ± 5	17 ± 2	46 ± 3	20 ± 6	67	10 ± 1	29 ± 7	11 ± 6	48 ± 11	90
	1050	17 ± 2	20 ± 3	37 ± 3	24 ± 2	65	20 ± 3	16 ± 3	30 ± 4	32 ± 3	88
	1350	20 ± 2	29 ± 2	24 ± 4	26 ± 4	47	18 ± 1	21 ± 1	33 ± 1	26 ± 2	59
Colored	100	33 ± 7	30 ± 3	19 ± 3	18 ± 5	45	41 ± 4	24 ± 3	14 ± 2	22 ± 4	49
	200	31 ± 7	20 ± 3	38 ± 4	12 ± 4	48	26 ± 2	13 ± 1	33 ± 4	28 ± 3	49
	300	25 ± 3	14 ± 4	36 ± 3	25 ± 2	49	26 ± 3	19 ± 4	26 ± 4	29 ± 4	50
	400	19 ± 3	23 ± 3	27 ± 3	32 ± 4	49	16 ± 2	15 ± 3	33 ± 3	37 ± 3	60
	880	22 ± 3	17 ± 4	28 ± 4	33 ± 1	49	13 ± 3	24 ± 5	26 ± 4	36 ± 5	66
	1050	18 ± 3	27 ± 3	20 ± 2	34 ± 4	48	11 ± 2	20 ± 3	38 ± 2	31 ± 2	68
	1350	26 ± 3	16 ± 3	29 ± 1	29 ± 3	48	15 ± 2	20 ± 4	34 ± 5	31 ± 5	58

The column denoted ϕ_A^E indicates the experimental findings of Broda.[66] The discrepancy between the ϕ_A and ϕ_A^E columns is a direct consequence of the transformation of the experimental data in eq. (11).

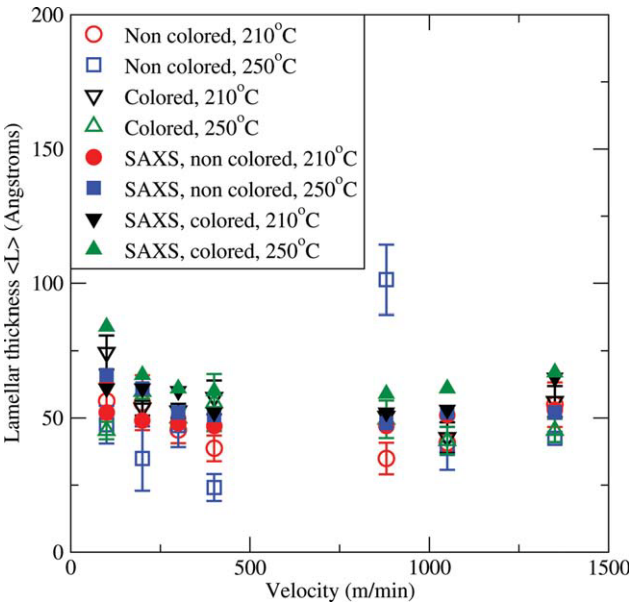

Figure 2 $\langle L \rangle$ obtained from simulated annealing as a function of take-up velocity (open symbols). Also shown are the results obtained with independent SAXS measurements (filled symbols).[66] [Color figure can be viewed in the online issue, which is available at www.interscience.wiley.com.]

The second set of data with which we chose to compare our analysis technique was published by Mezghani and Phillips.[34] In these experiments, iPP was supplied by Exxon Corp. and had structural irregularities of 1.26%. These specimens were loaded into a pressure chamber and heated to 200°C and held at this temperature for 10 min. The temperature was reduced to the desired crystallization temperature, and a known pressure was applied. This study yielded several specimens, crystallized at two different pressures and multiple temperatures.

The WAXS diffractograms of these specimens were analyzed with simulated annealing. Figure 3 shows the phase content of the three phases as a function of crystallization temperature. The phase content of phase i was obtained as $\phi_i/(\phi_\alpha + \phi_\beta + \phi_\gamma)$. The results of simulated annealing indicated that, for both specimens, the γ phase was dominant and was present in excess of 50%. Specimens prepared at 125 MPa did not show an appreciable change in the phase content as a function of the crystallization temperature. Specimens prepared at 250 MPa showed an increase in γ content from 50 to 75%, accompanied by a corresponding decrease in the α and β phases from about 25% each to 12% each. This trend is consistent with previous observations.[53]

The average overall lamellar thickness obtained by the analysis of these data was in the range 50–100 Å. The values obtained with SAXS data, as reported in the original article,[34] were in the range 80–150 Å. Once again, the lamellar thickness values estimated by simulated annealing seemed somewhat lower than the values estimated by SAXS, which indicated that the experimental specimens might have contained some residual strain.

The fits obtained to the WAXS patterns published by Broda[66] are shown in Figures 4 and 5. The fits obtained to the WAXS patterns published by Mezghani and Phillips[34] are shown in Figure 6. In a majority of the specimens, the fitted curves agreed well with the experimental curve. In some cases, such as specimens 3–6 in Figure 4(b), there is some disparity between the fitted and experimental curves. Possible sources of error include minute errors in the crystal structure of the ideal phases, possible instrument error, and parasitic scattering. However, despite this disparity, the lamellar thicknesses obtained seem realistic and are in agreement with the lamellar thicknesses obtained with SAXS. Also, the trend of dominant γ content for specimens prepared at high pressures was also observed in the results from simulated annealing.

The overall lamellar thickness obtained in this study is in surprisingly good agreement with the lamellar thickness obtained with SAXS. As stated earlier, the method used in this study does not explicitly consider the line broadening resulting from lattice strain, but lumps this effect along with line broadening resulting from finite lamellar size. This

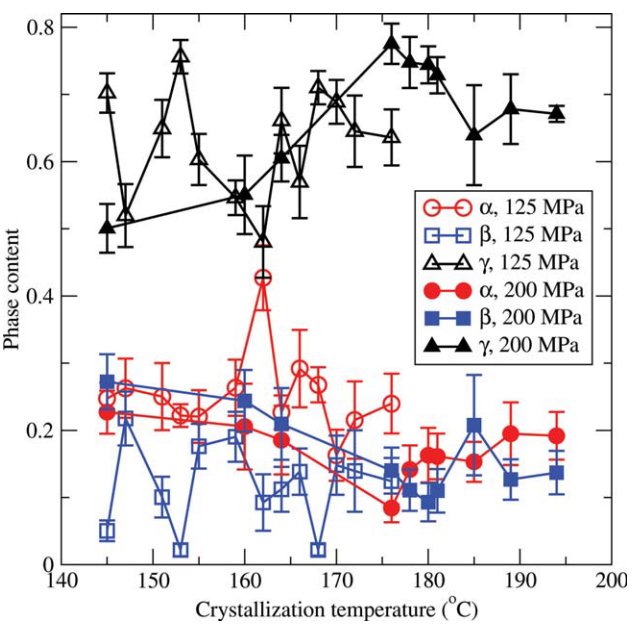

Figure 3 Phase content of iPP crystallized at various temperatures and pressures obtained with simulated annealing on the WAXS data presented by Mezghani and Phillips.[34] The γ phase is dominant in both specimens. Specimens prepared at 200 MPa showed an increase in γ content with increasing crystallization temperature. [Color figure can be viewed in the online issue, which is available at www.interscience.wiley.com.]

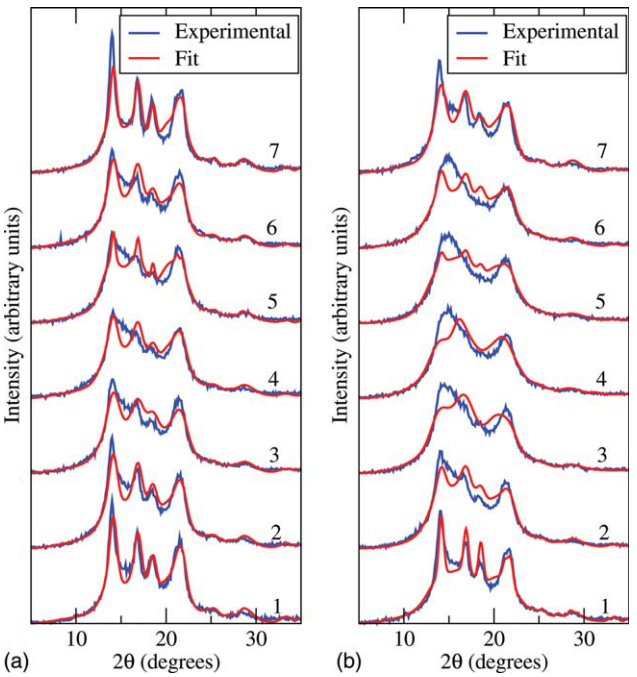

Figure 4 Fits to the experimental data from Broda[66–68] for noncolored iPP fibers (a) extruded at 210°C and (b) extruded at 250°C at different velocities: (1) 100, (2) 200, (3) 300, (4) 400, (5) 880, (6) 1050, and (7) 1350 m/min. [Color figure can be viewed in the online issue, which is available at www.interscience.wiley.com.]

leads to an underestimation of the actual lamellar thickness. The separation of line broadening into contributions from lattice strain and finite lamellar thickness remains an open question. In addition to the overall lamellar thickness, simulated annealing predicts an average lamellar thickness for each individual phase. At the time of this writing, we are not aware of an experimental method that can measure the lamellar thickness of individual phases in a mixture and, thus, are unable to validate this finding.

Although the results obtained with simulated annealing seems largely reasonable, it is important to point out some of the limitations and outstanding issues. K used in eq. (5) was taken to be 0.93, from Scherrer's original work.[56,57] It is possible that for analyzing iPP, a different value of K is the more proper one. A different value of K, used in conjunction with a different value of L that maintains the ratio K/L, does not affect the full width at half-maximum (w) of a peak. Thus, a different value of K is expected to correspondingly change the value of L, whereas when the phase content obtained from simulated annealing is left unchanged, as w depends on the ratio K/L.

The crystallinity obtained from simulated annealing was in the range 52–88%. These values are somewhat higher than the typical crystallinity values seen in the literature. This is a direct consequence of the baseline correction used in this study to account for the arbitrary shift factors used in publishing WAXS data. With a WAXS diffractogram corrected only for the fixed background intensity that is obtained from scattering by air, further baseline correction becomes unnecessary, and a more accurate value of crystallinity may be obtained. At the time of this writing, we are not aware of any published experimental data that has been corrected only for background scattering. Since the scope of this study was to establish the computational framework, we feel that further experimental studies would be required to address the issue. The accuracy of predicted crystallinity also depends on the accuracy of the WAXS pattern of a purely amorphous specimen, and there is a certain amount of difficulty associated with obtaining a purely amorphous specimen of iPP.[69]

Simulated annealing aims to find a single point in the phase space $S(\phi_\alpha,\phi_\beta,\phi_\gamma,\phi_A,L_\alpha,L_\beta,L_\gamma)$ that minimizes E defined in eq. (6). In principle, there can exist multiple, widely separated points in phase space that yield comparable values of E. In other words, given an experimental WAXS pattern, two widely different crystalline phase contents and lamellar thicknesses may be obtained that fit the experimental data. Such a situation would occur if the peaks of the ideal crystalline phases are all close to each other. Fortunately, in the case of iPP, even

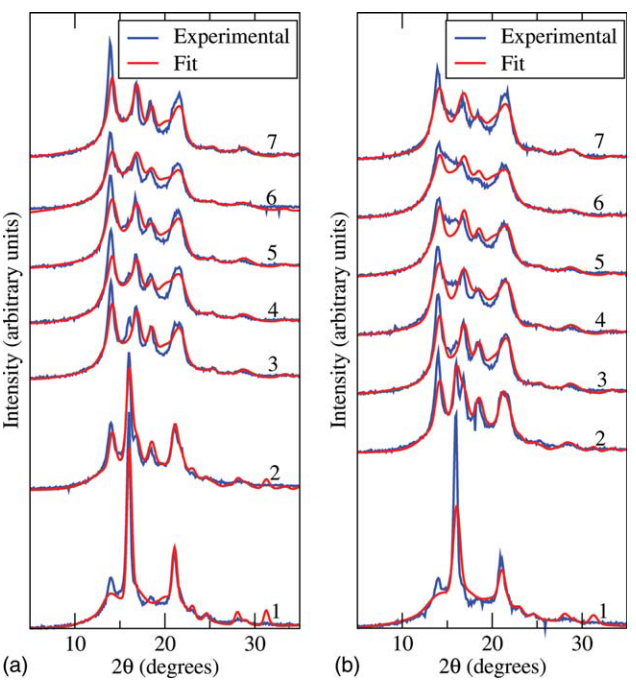

Figure 5 Fits to the experimental WAXS data from Broda[66–68] for iPP fibers colored with quinacridone pigments (a) extruded at 210°C and (b) extruded at 250°C at different velocities: (1) 100, (2) 200, (3) 300, (4) 400, (5) 880, (6) 1050, and (7) 1350 m/min. [Color figure can be viewed in the online issue, which is available at www.interscience.wiley.com.]

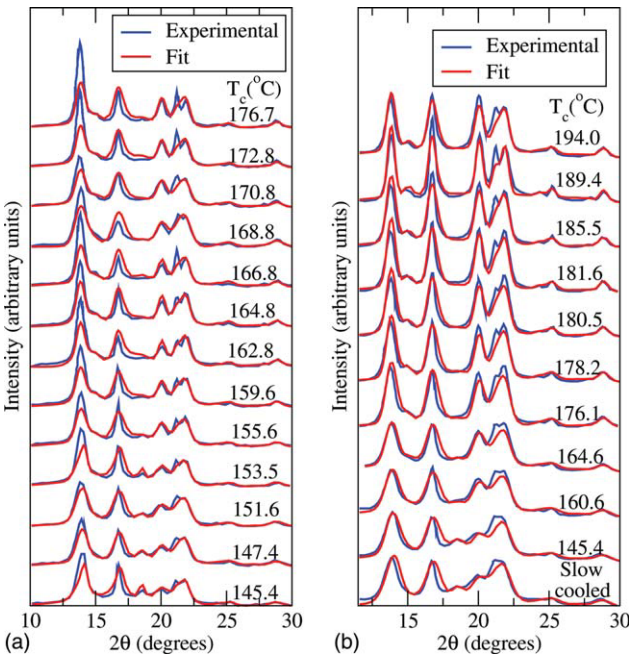

Figure 6 Fits to the experimental data from Mezghani et al.[34] for iPP crystallized isothermally at (a) 125 and (b) 200 MPa at various temperatures. The crystallization temperatures are indicated in the figure. [Color figure can be viewed in the online issue, which is available at www.interscience.wiley.com.]

though some peaks of each crystalline phase are close to the peaks of other crystalline phases, each crystalline phase has at least one distinct peak that was not present in any of the other crystalline phases. Indeed, examining Table I, we see that both the α and γ phases have high-intensity peaks at 14.1 and 13.8°, and all three phases have moderate intensity peaks in the vicinity of 21.2°. Nevertheless, each phase has its own distinct peak (α at 18.55°, β at 16.05°, and γ at 20.07°) of relatively high intensity. Thus, for example, when one analyzes a specimen rich in γ content, choosing a point in phase space that is γ deprived yields a large value of E and, thereby, forces the search algorithm to move toward γ-rich points. It is this feature of iPP that allows simulated annealing to find solutions in phase space that are close to each other, and we expect the algorithm to yield better results for polymers that have high-intensity peaks that are widely separated on the 2θ axis.

CONCLUSIONS

A novel method of simultaneously estimating the phase content and lamellar thickness of each phase in iPP from WAXS data was presented. This method is intended as an analysis technique for polymers whose ideal crystalline and amorphous structures are well known. Under the assumption that WAXS data may be decomposed into a weighted sum of its constituent elements, the weighting factors of the constituent elements were determined with a Monte Carlo technique. The average lamellar thickness measured with simulated annealing was slightly lower than the value measured by other techniques, such as SAXS. This was because, in the simulated annealing algorithm, lattice-strain-induced line-broadening effects are combined with lamellar-thickness-induced line broadening. This method also yields the average lamellar thickness of each individual phase, but this part of the study needs experimental validation. The method presented in this article is general enough to be extended to other polymer systems, copolymers, and polymer blends where the constituents of the mixture yield WAXS patterns that are clearly distinguishable.

Partial support for this work was provided by Procter & Gamble Co. The authors thank Jan Broda from the University of Bielsko Biala, Poland, for sharing his WAXS data.

References

1. Isasi, J. R.; Haigh, J. A.; Graham, J. T.; Mandelkern, L.; Alamo, R. G. Polymer 2000, 41, 8813.
2. Strobl, G. R.; Schneider, M. J Polym Sci Polym Phys Ed 1980, 18, 1343.
3. Mandelkern, L. Polym J 1985, 17, 337.
4. Farrow, G.; Ward, I. M. Polymer 1960, 1, 330.
5. Nishida, K.; Konishi, T.; Kanaya, T.; Kaji, K. Polymer 2004, 45, 1433.
6. Way, J. L.; Atkinson, J. R. J Mater Sci 1971, 6, 102.
7. Bessell, T. J.; Hull, D.; Shortall, J. B. J Mater Sci 1975, 10, 1127.
8. Schultz, J. M. Polym Eng Sci 1984, 24, 770.
9. Yeh, J. T.; Runt, J. J Mater Sci 1989, 24, 2637.
10. Sue, H.; Earls, J.; Hefner, R. J Mater Sci 1997, 32, 4031.
11. Park, S. D.; Todo, M.; Arakawa, K.; Koganemaru, M. Polymer 2006, 47, 1357.
12. Grzybowski, S.; Zubielik, P.; Kuffel, E. IEEE Trans Power Delivery 1989, 4, 1507.
13. Tanaka, T. IEEE Trans Electr Insul 1992, 27, 424.
14. Zhou, Y.; Wang, N. H.; Yan, P.; Liang, X. D.; Guan, Z. C. J Electrostat 2003, 57, 381.
15. Tanaka, T.; Montanari, G. C.; Mulhaupt, R. IEEE Trans Dielectr Electr Insul 2004, 11, 763.
16. Nakagawa, T.; Nakiri, T.; Hosoya, R.; Tajitsu, Y. IEEE Trans Ind Appl 2004, 40, 1020.
17. Zhou, H.; Wilkes, G. L. Polymer 1997, 38, 5735.
18. Ihn, K. J.; Tsuji, M.; Kawaguchi, A.; Katayama, K. Bull Inst Chem Res Kyoto Univ 1990, 68, 30.
19. Sohn, B. H.; Yun, S. H. Polymer 2002, 43, 2507.
20. Xia, Z.; Sue, H. J.; Wang, Z.; Avila-Orta, C. A.; Hsiao, B. S. J Macromol Sci Phys 2001, 40, 625.
21. Wang, Z. G.; Hsiao, B. S.; Fu, B. X.; Liu, L.; Yeh, F.; Sauer, B. B.; Chang, H.; Schultz, J. M. Polymer 2000, 41, 1791.
22. Marega, C.; Marigo, A.; Cingano, G.; Zannetti, R.; Paganetto, G. Polymer 1996, 37, 5549.
23. Somani, R. H.; Hsiao, B. S.; Nogales, A.; Srinivas, S.; Tsou, A. H.; Sics, I.; Balta-Calleja, F. J.; Ezquerra, T. A. Macromolecules 2000, 33, 9385.
24. Trifonova, D.; Varga, J.; Vancso, G. J. Polym Bull 1998, 41, 341.
25. Li, L.; Chan, C. M.; Yeung, K. L.; Li, J. X.; Ng, K. M.; Lei, Y. Macromolecules 2001, 34, 316.

26. Reiter, G.; Castelein, G.; Sommer, J. U. Phys Rev Lett 2000, 86, 5918.
27. Takahashi, Y.; Tadokoro, H. Macromolecules 1973, 6, 672.
28. Lightfoot, P.; Mehta, M. A.; Bruce, P. G. Science 1993, 262, 883.
29. Lotz, B.; Wittmann, J. C. Polymer 1996, 37, 4979.
30. Dorset, D.; McCourt, M.; Kopp, S.; Schumacher, M.; Okihara, T.; Lotz, B. Polymer 1998, 39, 6331.
31. Meille, S. V.; Bruckner, S.; Porzio, W. Macromolecules 1990, 23, 4114.
32. Fontana, L.; Vinh, D. Q.; Santoro, M.; Scandolo, S.; Gorelli, F. A.; Bini, R.; Hanfland, M. Phys Rev B 2007, 75, 174112.
33. Mezghani, K. Polymer 1997, 38, 5725.
34. Mezghani, K.; Phillips, P. J. Polymer 1998, 39, 3735.
35. Jones, A. T.; Aizlewood, J. M.; Becket, D. R. Makromol Chem 1964, 75, 134.
36. Ruland, W. Acta Crystallogr 1961, 14, 1180.
37. Ruland, W. Polymer 1964, 5, 89.
38. Vonk, C. G. J Appl Crystallogr 1973, 6, 81.
39. Kavesh, S.; Schultz, J. M. J Polym Sci Part A-2: Polym Phys 1971, 9, 85.
40. Isasi, J. R.; Mandelkern, L.; Galante, M. J.; Alamo, R. G. J Polym Sci Part B: Polym Phys 1999, 37, 323.
41. Mo, Z.; Zhang, H. J. Macromol Sci Rev Macromol Chem Phys 1995, 35, 555.
42. Weidinger, A.; Hermans, P. H. Makromol Chem 1961, 50, 98.
43. Quynn, R. G.; Riley, J. L.; Young, D. A.; Noether, H. D. J Appl Polym Sci 1959, 2, 166.
44. Farrow, G. Polymer 1961, 2, 409.
45. Natta, G.; Corradini, P.; Cesari, M. R C Accad Lincei 1957, 22, 11.
46. Krache, R.; Benavente, R.; Lopez-Majada, J. M.; Perena, J. M.; Cerrada, M. L.; Perezet, E. Macromolecules 2007, 40, 6871.
47. Nedkov, E.; Dobreva, T. Eur Polym J 2004, 40, 2573.
48. Busse, K.; Kressler, J. Macromolecules 2000, 33, 8775.
49. Addink, E. J.; Bientema, J. Polymer 1961, 2, 185.
50. Mansel, S.; Pérez, E.; Benavente, R.; Pereña, J. M.; Bello, A.; Röll, W.; Kirsten, R.; Beck, S.; Brintzinger, H.-H. Macromol Chem Phys 1999, 200, 1292.
51. Awaya, H. Polymer 1988, 26, 591.
52. Meille, S.; Bruckner, S. Nature 1989, 340, 455.
53. Campbell, R. A.; Philips, P. J. Polymer 1993, 34, 4809.
54. Suhm, J. J Mater Chem 1998, 8, 553.
55. Accelrys. Materials Studio Overview. http://accelrys.com/products/materials-studio (accessed Jan 2010).
56. Scherrer, P. Göttinger Nachr Ges 1918, 2, 98.
57. Patterson, A. L. Phys Rev 1939, 56, 978.
58. Cullity, B. D.; Stock, S. R. Elements of X-Ray Diffraction; Pearson: Parsippany, NJ, 2001.
59. Klug, H. P. X-Ray Diffraction Procedures; Wiley: New York, 1974.
60. Sanchez-Bajo, A.; Cumbrera, F. L. J Appl Crystallogr 1997, 30, 427.
61. Wang, H.; Zhou, J. J Appl Crystallogr 2005, 38, 830.
62. Kirkpatrick, S.; Gelatt, C. D.; Vecchi, M. P. Science 1983, 220, 671.
63. Yan, S.; Petermann, J.; Yang, D. Polym Bull 1997, 38, 87.
64. Maiti, P.; Hikosaka, M.; Yamada, K.; Toda, A.; Gu, F. Macromolecules 2000, 33, 9069.
65. Hosier, I. L.; Alamo, R. G.; Lin, J. Polymer 2004, 45, 3441.
66. Broda, J. J Appl Polym Sci 2003, 89, 3364.
67. Broda, J. Polymer 2003, 44, 1619.
68. Broda, J. Cryst Growth Des 2004, 4, 1277.
69. Davies, R. J.; Zafeiropoulos, N. E.; Schneider, K.; Roth, S. V.; Burghammer, M.; Riekel, C.; Kotek, J. C.; Stamm, M. Colloid Polym Sci 2004, 282, 854.